Pulse Radiation Characteristics Prediction Method of Vivaldi Antenna based on Dipole Array

Binwen Wang, Hui Ning, Hao Cai, Qilong Liu, Yan Wang, and Youjie Yan

Northwest Institute of Nuclear Technology
Xi'an 710024, China
srxh_bingwen@aliyun.com, ninghuisun@aliyun.com, 1178818032@qq.com, 820091469@qq.com,
1278206596@qq.com, pine976@163.com

Abstract – This paper presents a theoretical method to estimate the pulse radiation characteristics of Vivaldi antennas. Based on the surface current distribution and the ultra-wideband radiation principle, Vivaldi antenna is equivalently modeled as a dipole array, and the pulse radiation characteristics of a single Vivaldi antenna are brought out utilizing the spatial superposition approach. Then, the influences and results of the Vivaldi antenna pulse characteristics prediction with different construction ways of the dipole array and element numbers are furthermore investigated. Next, a quadratic spatial superposition technique is employed to complete the theoretical prediction for time-domain radiation characteristics of Vivaldi antenna arrays. Experiments and simulations are conducted separately to verify the proposed method for both single Vivaldi antenna and array. The validated results demonstrate that the dipole array-based theoretical prediction method can effectively capture the pulse radiation characteristics for both individual Vivaldi antenna and array operating in different modes, thereby addressing challenges associated with estimating radiation characteristics in ultra-wideband pulse applications.

Index Terms – Antenna array, beam scanning, dipole array, pulse radiation characteristics, Vivaldi antenna.

I. INTRODUCTION

The Vivaldi antenna, also known as the tapered slot antenna, is a planar end-fire antenna initially proposed by Gibson in 1979 [1]. Owing to its exceptional characteristics of ultra-wideband operation, high gain, low profile and excellent directivity, it has garnered significant attention and extensive applications in the field of radio communication technology [2–10]. Particularly, the attributes of stable phase center behavior, easy integration capability and cost-effectiveness exhibited by the Vivaldi antenna render it highly suitable for time domain radiation applications such as through-wall radar [11–12], ground-penetrating radar [13–14], non-destructive

testing [8, 15] and biomedical imaging [16–18]. In comparison to traditional pulse radiation antennas like TEM horn antennas [19–20] or IRA [21–22], the Vivaldi antenna offers numerous advantages. Furthermore, akin to most antennas, Vivaldi antenna can be employed as array elements. Radiation gain enhancement can be achieved while enabling functionalities like beamforming and beam-scanning through precise control of excitation timing [23–34]. However, despite the remarkable advantages mentioned above, this type of antenna also encounters several technical challenges. Foremost among them is accurately calculating the radiation characteristics of Vivaldi antenna array in time domain. The absence of clear field distribution function poses difficulties for large-scale synthesis and beamforming operations on Vivaldi antenna arrays [25], thereby significantly limiting the engineering realization and practical application.

The computational electromagnetics methods and commercial electromagnetic simulation software can accurately compute the radiation characteristics of the array antennas [26–28]. However, when dealing with very short excited pulses and excessively large array scales, the computation grid number becomes too large, leading to significant consumption of computing resources and time due to limitations in computer hardware conditions. Consequently, the calculation efficiency becomes extremely low or even impractical. In order to address this challenging issue associated with calculating radiation characteristics for large-scale array antennas, Pozar proposed the active element pattern method [29], which predicts the total radiation field by combining the active patterns of each array element using superposition principles. Building upon this approach, Yang introduced the subarray equivalent extrapolation method [30] to enhance computational efficiency for determining array antenna radiation characteristics. Zhang et al. applied the active element pattern method to calculate time-domain patterns for TEM horn antenna arrays [31]. Although widely utilized and validated, employing the

active element pattern method requires extensive data measurement efforts that are labor-intensive, costly and tedious. Additionally, when there are changes in excitation pulse waveforms, re-measurements become necessary. Theoretical predictions have also been explored in relevant studies. For instance, Mikheev et al. derived an electric field calculation formula based on electromagnetic tensor methods for arbitrary wire antennas [32], enabling prediction of radiation characteristics for wire antenna arrays through superposition principles. Reference [33] has employed multiple reflection theory-based estimations to determine time-domain radiation characteristics of bowtie antennas. Theoretical methods, however, are confined to a subset of radiating antennas with relatively simplistic structures that lend themselves to analytical solutions.

To summarize, the theoretical prediction method stands out as the most cost-effective and ideal approach, primarily based on calculating the time-domain radiation field of a single antenna and employing spatial superposition principles. The spatial superposition process takes into account the influence of array factors, thereby eliminating the need for additional extraction of array factor. Therefore, accurately predicting the radiation characteristics of an array antenna in the time domain hinges upon precisely calculating the radiation field of the array element. This paper proposes a dipole array-based theoretical method for predicting radiation characteristics of Vivaldi antennas and their array in time-domain, building upon surface current distribution and wideband radiation principles, and verified by experiments and numerical simulation. This paper is organized as follows. The first section is the introduction, the second section outlines prediction concepts and implementation processes, the third section presents the verification, and the final section is the conclusion.

II. PREDICTION METHOD

Figure 1 illustrates the typical Vivaldi antennas, coplanar Vivaldi and antipodal Vivaldi [34], respectively. The sole distinction lies within the feeding structures, while the radiation principle remains unaltered. In accordance with the theory of time-domain electromagnetics, the pulse radiation characteristics of the antenna can be acquired utilizing the Maxwell's equations and time-domain retarded potential after determining the antenna surface current distribution. However, for most UWB pulse radiating antennas, the time-domain surface current distribution is so complicated that there are challenges in providing an analytical solution. Therefore, it is imperative to reasonably approximate and solve for the current distribution in order to address this prediction problem.
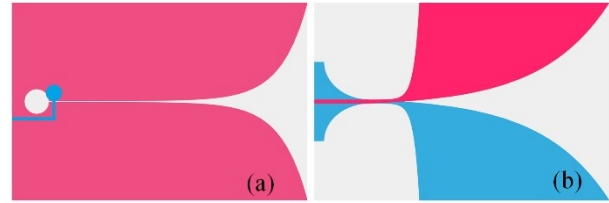

Fig. 1. Typical Vivaldi antennas: (a) coplanar Vivaldi and (b) antipodal Vivaldi.

Firstly, the investigation focuses on the antenna surface current distribution. Figure 2 illustrates the current distribution at typical frequency points of the two Vivaldi antennas, obtained using the time-domain finite integral techniques.
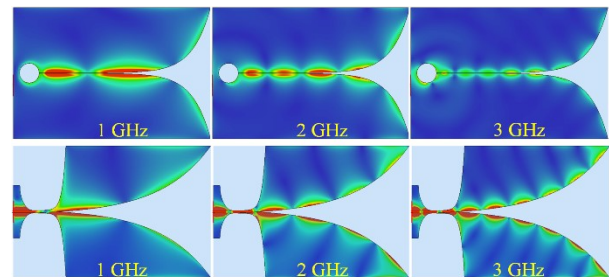

Fig. 2. Current distributions of the Vivaldi antennas in typical frequency points.

Figure 2 qualitatively demonstrates that the surface current of the Vivaldi antenna is primarily concentrated along the exponential gradient edge of the radiation patch, with minimal contribution from other positions on the patch. Consequently, it can be inferred that the primary path of the surface current flow corresponds to this exponential gradient line. Therefore, the Vivaldi antenna can be considered as a curvilinear radiator composed of two exponential gradient lines, as illustrated in Fig. 3.

The simplification of the solution difficulty is greatly facilitated by the equivalence based on surface current distribution. Upon examining the operating principle and radiation process of Vivaldi antenna, it becomes apparent that the ultra-wideband feature stem from the varied length between the gradient slots, radiating electromagnetic waves with distinct wavelengths while preserving relatively stable phase centers [35]. Thus, the equivalent curvilinear radiator shown in Fig. 3 can be further modeled by a dipole antenna array, as plotted in Fig. 4.

In order to elucidate the estimation idea more clearly, Fig. 4 only employs an array consisting of three dipole elements to simulate the Vivaldi antenna. It is worth noting that the array with multiple elements can also be utilized, wherein the curvilinear radiator is
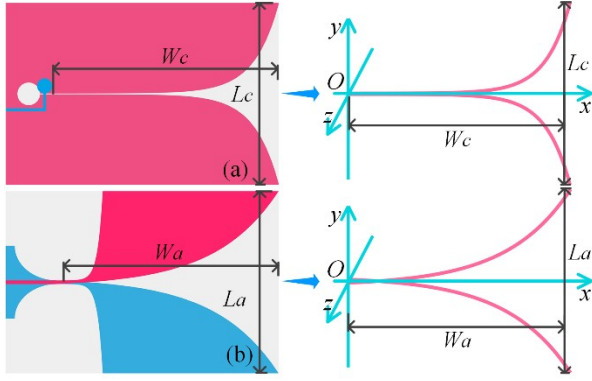
Fig. 3. Vivaldi antennas and the equivalent curvilinear radiators: (a) coplanar Vivaldi and (b) antipodal Vivaldi.
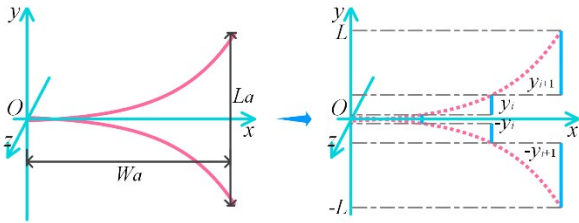

Fig. 4. Utilizing the dipole array to model the curvilinear radiator and the primary path of the surface current flow.

of the curvilinear radiator are opposite, and the contribution to the field on the yoz plane is zero. For other field points, the contribution of the x component remains negligible.

The above-mentioned equivalence simplifies the radiation characteristics prediction of the Vivaldi antenna to the calculation of the radiated field of a dipole array in time-domain, the foundation of which is the pulse radiation of a single dipole antenna. Figure 5 illustrates the radiation process of the dipole antenna, which is positioned along the y axis. To differentiate the source point and field point, the coordinates of source points are attached by a superscript s.
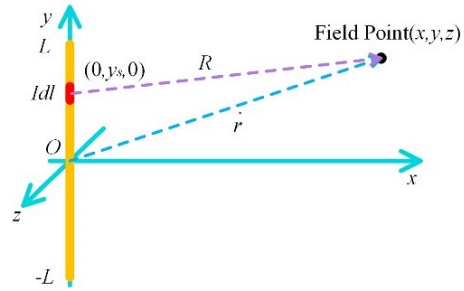

Fig. 5. Radiation process of the dipole antenna.

divided into several segments and each segment corresponds to an equivalent dipole antenna at the respective position. However, it should be emphasized that this dipole array differs from the conventional arrays in terms of the spatial distribution of the array elements, which follows the exponential gradient lines of the Vivaldi antenna. Moreover, unlike independently feeding elements in traditional arrays, current propagates along the previous dipole element towards the end and then continues into the subsequent dipole element. The total length of all elements of the dipole array matches that of the dimensions in the E-plane of the Vivaldi antenna. Overall, this equivalence effectively divides a dipole antenna with the length identical to the E-plane size of Vivaldi antenna into smaller dipoles, distributed according to the exponential gradient line structure characteristics of Vivaldi antenna. From the perspective of current element, when the element number of the dipole array is sufficient, the dipole array can be regarded as a collection of current elements, which is equal to solve the radiation characteristics of Vivaldi antenna utilizing the current element analysis. In fact, the Vivaldi antenna is considered as the dipole array in y direction, disregarding the x component current of the curvilinear radiator. This is because, from an external viewpoint, the current flows in the x-direction on the upper and lower poles

According to the theory of multiple reflections, the frequency domain current distribution of dipole antenna can be elegantly expressed as [36]:

$$\overrightarrow{I}(l,\omega) = I_0(\omega)\frac{e^{-jkl}+\Gamma_2 e^{-jk(2L-l)}}{1-\Gamma_1\Gamma_2 e^{-jk2L}}, \quad (1)$$

where I_0 represents the amplitude of excitation current, k is the propagation constant, l refers to the distance between the current element and the feeding point of dipole, L denotes the length of dipole arm, and Γ_1 and Γ_2 stand for the reflection coefficients at the feeding and terminal end, respectively.

The current distribution reveals that the magnetic vector potential in the y-direction at the field point $\overrightarrow{r}$ is:

$$\overrightarrow{A}(\overrightarrow{r},\omega) = \frac{\mu_0 I_0(\omega)}{4\pi}\int_{2L}\frac{e^{-jkl}+\Gamma_2 e^{-jk(2L-l)}}{1-\Gamma_1\Gamma_2 e^{-jk2L}}\frac{e^{-jkR}}{R}dl, \quad (2)$$

where R is the distance between field and source points:

$$R = \sqrt{(x-x_s)^2+(y-y_s)^2+(z-z_s)^2}\Big|_{x_s=0,z_s=0}^{\text{for dipole}}. \quad (3)$$

The magnetic field at the field point can be derived from equation (2), thereby enabling us to ascertain the components of the electric field in each direction:

$$\overrightarrow{E}\left(\overrightarrow{r},\omega\right)_x = \frac{I_0\left(\omega\right)\left(x-x_s\right)}{j4\pi\omega\varepsilon_0}\int_{-L}^{L} i(R,l)\left(y-y_s\right)a_R dl, \tag{4}$$

$$\begin{aligned}\vec{E}(\vec{r},\omega)_y =\;& \frac{I_0(\omega)}{j2\pi\omega\varepsilon_0}\int_{-L}^{L} i(R,l)b_R dl \\ & -\frac{I_0(\omega)z^2}{j4\pi\omega\varepsilon_0}\int_{-L}^{L} i(R,l)a_R dl \\ & -\frac{I_0(\omega)\left(x-x_s\right)^2}{j4\pi\omega\varepsilon_0}\int_{-L}^{L} i(R,l)a_R dl,\end{aligned} \tag{5}$$

$$\overrightarrow{E}\left(\overrightarrow{r},\omega\right)_z = \frac{I_0\left(\omega\right)z}{j4\pi\omega\varepsilon_0}\int_{-L}^{L} i(R,l)\left(y-y_s\right)a_R dl, \tag{6}$$

where the mentioned functions are designated as:

$$\begin{cases} i(R,l) = \dfrac{e^{-jk(R+l)}+\Gamma_2 e^{-jk(2L+R-l)}}{1-\Gamma_1\Gamma_2 e^{-jk2L}} \\ a_R = -k^2 R^{-3}+3jkR^{-4}+3R^{-5} \\ b_R = jkR^{-2}+R^{-3} \end{cases}. \tag{7}$$

By performing the inverse Fourier transform on equations (4-6), the corresponding radiation field in time-domain of the dipole antenna can be acquired, and the electric field in *y* direction is the principle polarized component, which is the subsequent focus to be investigated.

A simple verification to the theoretical calculation of the radiation field for dipole antenna is presented below, employing the time-domain finite integral techniques. As marked in Fig. 5, a dipole is positioned along the *y* direction with the pole length of 15 cm and the feeding gap of 4 mm. Utilizing a Gaussian pulse with pulse width of 0.6 ns shown in Fig. 6 as the excitation, the principle polarized electric field at the field point (5,0,0) is obtained, as plotted in Fig. 7.
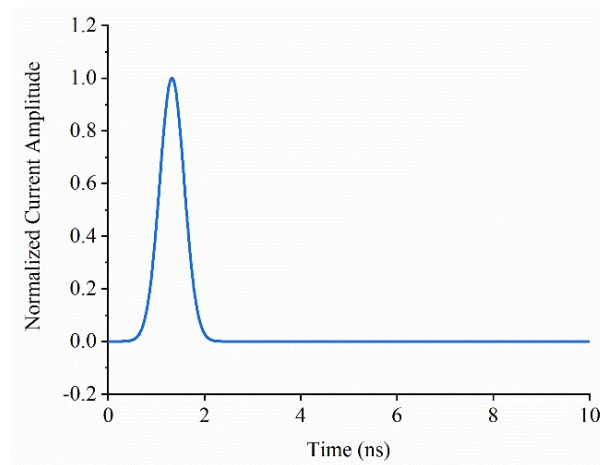

Fig. 6. Excitation pulse with pulse width of 0.6 ns.

The radiated electric field waveforms of the dipole antenna obtained by the prediction method, as depicted
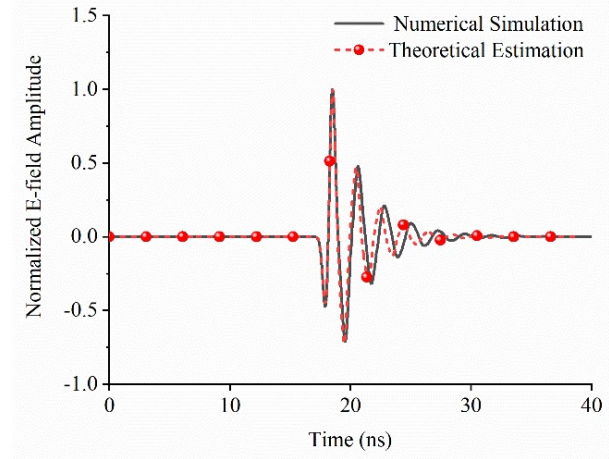

Fig. 7. The normalized principle polarized electric field waveform at the field point (5,0,0).

in Fig. 7, exhibits remarkable concordance with the numerical results with the pulse mean square error of 0.43. Only a slight discrepancy in pulse duration is observed. This variation is primarily attributed to the pole radius of the dipole. Current concentration occurs along the dipole axis during the equivalence process, while the practical current is distributed across the dipole surface, thereby inducing a certain degree of broadening on the radiated electric field waveform.

The pulse radiation characteristics of a dipole array can be obtained by combining the radiation field of a single dipole with the principle of spatial superposition. However, for the dipole antenna array proposed and constructed in this paper, slight deviations in the calculation of radiation field arise due to differences in feeding ways and structure. These deviations are manifested in the integral range. For the i_{th} element in Fig. 4, the integral range of [-*L*,*L*] in equation (5) should be replaced by [-y_{i+1},-y_i] and [y_i,y_{i+1}], while the pole length *L* remains unchanged. That means, the current distribution of the i_{th} element is equal to that on the corresponding position of the dipole with total length of 2*L*, reflections resulted by the feeding gap and the terminal end of the dipole with length of 2*L* has been taken into account. Moreover, the reflections present in the current distribution on the i_{th} element are generated by both the feeding gap of the first element dipole and the terminal end of the n_{th} element dipole. And the positional difference among array elements has already been considered through *R* in equation (5).

According to the radiation process, there exist two approaches for calculating the radiation field of the proposed dipole array. The first approach involves direct superposition, whereby the radiation field generated by each individual dipole element at the designated point is considered. Consequently, the overall radiation field of

the dipole array can be determined:

$$\overrightarrow{E}_a(\overrightarrow{r},t) = \sum_{i=1}^{n} \overrightarrow{E}_i(\overrightarrow{r}_i,t), \qquad (8)$$

where $\overrightarrow{r}_i$ refers to the position vector of the field point $\overrightarrow{r}$ relative to the feeding center of the i_{th} element.

A more sophisticated approach involves treating the dipole array as an individual dipole, thus solving the radiation field of each segment. Subsequently, spatial superposition is performed while considering the time delays determined by the actual distance between field and source point:

$$\overrightarrow{E}_a(\overrightarrow{r},t) = \sum_{i=1}^{n} \overrightarrow{E}_{di}(\overrightarrow{r},t-t_{di}), \qquad (9)$$

where t_{di} indicates the relative time delays of the array elements.

Take an antipodal Vivaldi antenna with the dimensions of 200 mm $\times$ 300 mm as an example. Figure 8 illustrates the antenna model and the excitation pulse with the upper frequency limit of 3 GHz.
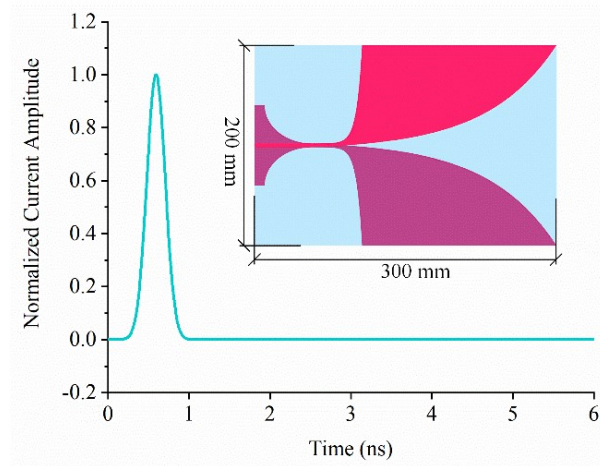

Fig. 8. Antipodal Vivaldi antenna and the excitation pulse.

Employing the aforementioned prediction method, the normalized electric field waveform in the principle polarized direction at the distance of 5 m along the main axis of the Vivaldi antenna is obtained, as depicted in Fig. 9. Subsequently, a comparison was made with the numerical results.

As observed in Fig. 9, the main pulse features of the predicted radiation waveform are in good agreement with the simulated results, except for a slight discrepancy in the tail oscillation. The corresponding pulse mean square error is 0.28. This can be attributed to the different treatment of the reflections at the feeding and terminal end in the simplified equivalent process, compared to the actual radiation. However, these predictions adequately meet the requirements for capturing the primary
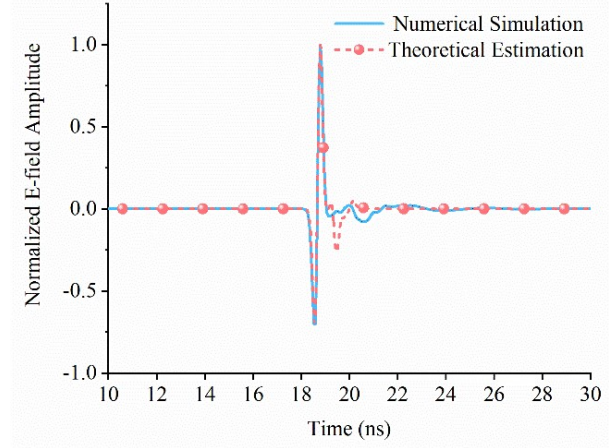

Fig. 9. Normalized radiated waveform at a distance of 5 m along the main axis of the Vivaldi antenna.

pulse characteristics. Furthermore, the impact of various dipole array elements on the radiation field of Vivaldi antenna is investigated. As depicted in Fig. 10, a comparative analysis is conducted to examine the predicted results of the radiation field with different dipole array elements.
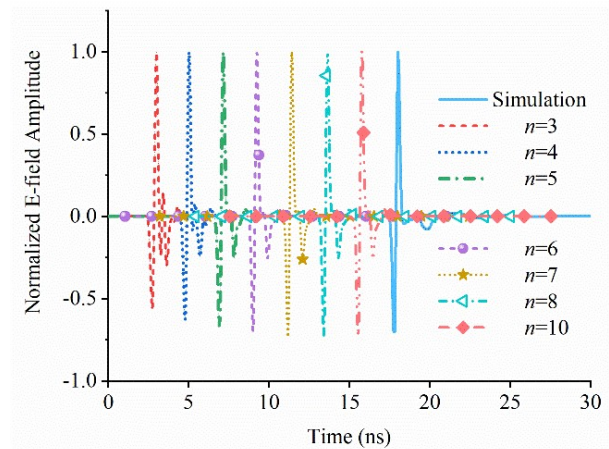

Fig. 10. Radiation field waveforms estimated by dipole array with different element numbers.

As illustrated in Fig. 10, the discrepancy between the theoretically estimated radiation waveforms and the numerical results diminishes with the increase of the dipole array element number, denoted as n. This convergence can be attributed to the increasing equivalence between the proposed dipole array and the gradient curve, aligning with expectations. It is well established that the time-domain radiation waveform of an antenna is determined by its current distribution. The duration of the radiation field waveform pulse is not only related

to the excitation pulse but also to the relative position of the current elements. As the number of equivalent dipole array elements increases, the positional equivalence becomes more pronounced. In essence, when the element number of the dipole array becomes sufficiently large, it approximates decomposing the gradient curve into an adequate number of elementary currents. It should be noted that a larger number of array elements leads to increased computational complexity, hence, the element number of the dipole array should be not overmuch in practical calculations and applications.

The dipole arrays utilized in the prediction process are uniform arrays with equidistant spacing along the x-axis. However, it is worth noting that non-uniform arrays can also be employed for an equivalent purpose. Figure 11 illustrates the schematic diagram of both a uniform dipole array and a non-uniform dipole array with the same element number of $n=6$. In the case of the non-uniform dipole array, the spacing along the x-axis adheres to a relationship of equal proportional variation, where q represents the common ratio.
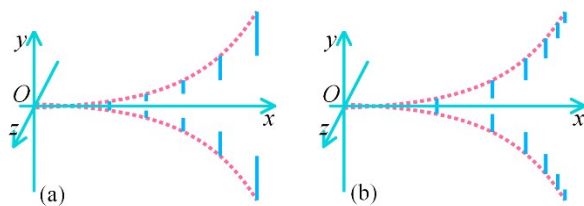

Fig. 11. Modeling methods of the curvilinear radiator: (a) uniform dipole array and (b) non-uniform dipole array.

The normalized radiation waveforms at the distance of 5 m along the main axis of the Vivaldi antenna obtained through the utilization of both uniform and non-uniform arrays is depicted in Fig. 12.

Figure 12 reveals that the non-uniform dipole array can also achieve a good prediction of Vivaldi antenna radiation field waveform. Specifically, for Vivaldi antennas, the initial section of the exponential gradient slot line primarily facilitates current propagation with minimal contribution to radiation, while it is the sharply changing length in y-direction in the end part of the exponential gradient slot line that plays a crucial role in generating radiation. In other words, the terminal part can be considered as the main radiating section. However, given that an excessive number of segments would lead to a significant increase in computational load, non-uniform segmentation allows for a more precise focus on the principal radiating components of the antenna. This precisely highlights the advantages offered by the non-uniform dipole array depicted in Fig. 11.

This section presents the concept and methodology of the dipole array-based prediction, while also analyz-
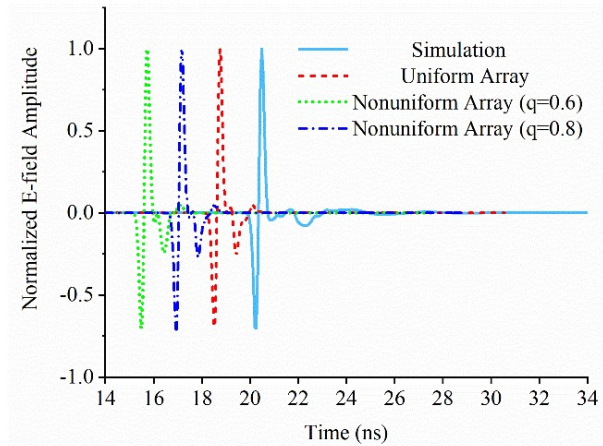

Fig. 12. Normalized radiated waveforms estimated by uniform dipole array and non-uniform dipole arrays.

ing the impact of array construction ways and element number on prediction effectiveness. Moreover, it should be noted that the discrete equivalent approach described herein can also be applied to antennas with more intricate structures as well as for estimating time domain radiation characteristics. In the following section, experiments and simulations are employed to further validate the prediction method.

III. VALIDATION AND DISCUSSION
A. Fabrication and measurement of antipodal Vivaldi

To validate the proposed theoretical prediction method, an antipodal Vivaldi antenna is designed and fabricated, as depicted in Fig. 13, which is printed on a FR-4 dielectric substance with thickness of 2 mm, relative dielectric constant of 4.3 and loss tangent of 0.025.

Firstly, the S11 of the antipodal Vivaldi antenna is measured within the frequency range of 10 MHz to 6 GHz, employing a vector network analyzer of KEYSIGHT E5080B. Figure 14 presents the measured curves, compared with numerical results obtained by finite integral techniques.
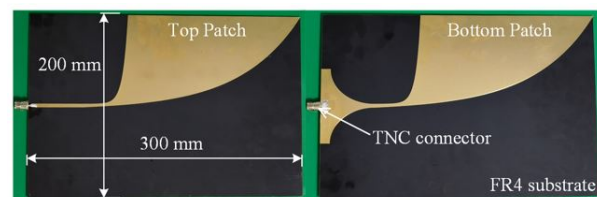

Fig. 13. The designed and fabricated antipodal Vivaldi antenna.

As depicted in Fig. 14, the measured results exhibit excellent agreement with the numerical simulations. The measured lower cut-off frequency (S11≤-10 dB) is 0.64
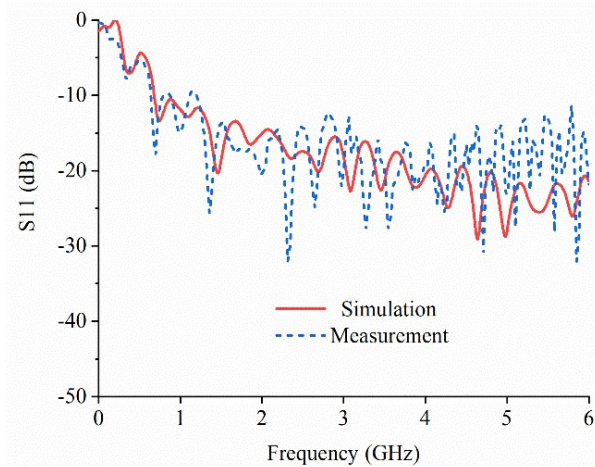
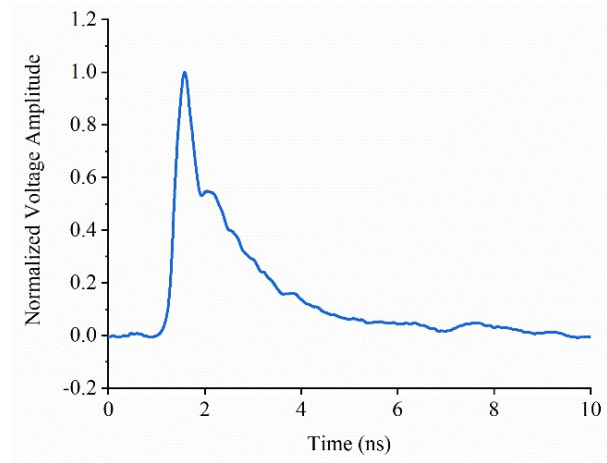Fig. 14. Comparison of the measured and simulated S11 parameter.

Fig. 15. The measured excitation pulse generated by the solid-state pulse generator.
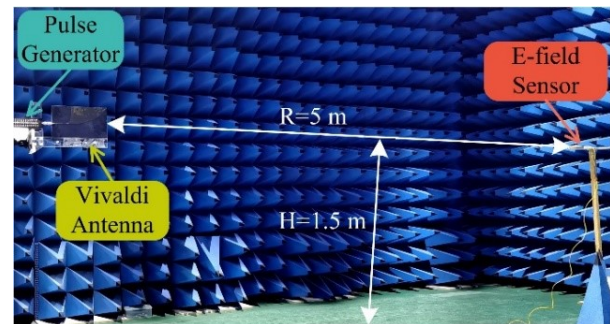

Fig. 16. Experimental setup for antipodal Vivaldi antenna.

Fig. 17. Comparison of the measured radiated field waveforms of Vivaldi antenna with theoretical prediction and numerical results.

GHz. Aperture width is about $0.43\lambda_0$ where λ_0 is the maximum operating wavelength. The measured frequency upper limit exceeds 6 GHz, resulting in a proportional bandwidth close to 10, proving that the fabricated antipodal Vivaldi antenna is a typical ultra-wideband antenna.

Secondly, the time-domain radiation characteristics of the antipodal Vivaldi antenna are demonstrated. The excitation pulses utilized in the second section are all ideal Gaussian pulses, which is too difficult to implement. Hence, an ultra-wideband solid-state pulse generator based on avalanche transistor is designed and employed to output the excitation pulse for the Vivaldi antenna. The measured excitation pulse is shown in Fig. 15. Then, a testing apparatus is established to measure the radiation field waveform of the antipodal Vivaldi antenna. Figure 16 illustrates the experimental setup. The antipodal Vivaldi antenna is feeding via TNC coaxial cable which is connected to the solid-state pulse generator. The field measurement system comprises a monopole probe and photoelectric module with the bandwidth up to 3 GHz and response time less than 150 ps. An oscilloscope of TELEDYNE LECROY 806Zi-B with the bandwidth of 6 GHz and sampling rater of 20 GSa/s is utilized. The measured radiation field waveform at the distance of 5 m along the main axis of the antenna is presented in Fig. 17, which is compared against theoretical estimation and numerical results.

As observed from Fig. 17, the radiated electric field waveforms are bipolar pulses under the excitation of the pulse depicted in Fig. 15. It is evident that the measured bipolar pulse accurately matches both the numerical and theoretical estimated results, demonstrating the effectiveness of the proposed prediction method for Vivaldi antenna radiation field. Comparatively speak-

ing, there are no related studies on the prediction of the radiated electric field for Vivaldi antenna in previous references, which further emphasizes the innovation
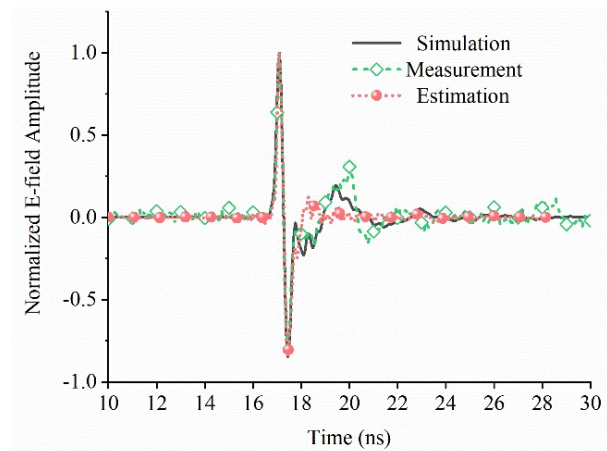
and significance of this work. Additionally, the proposed method and the conducted work in this paper offer a novel approach to analyze Vivaldi antennas. For instance, the theoretical prediction method enables quick examination of the impact of antenna dimensions on the radiation field, which is beneficial for antenna design and UWB pulse generator development. The time-domain pattern of single Vivaldi antenna is not particularly significant and was not elaborated here. In the subsequent section, the temporal pattern of the Vivaldi array will be analyzed and predicted.

B. Antipodal Vivaldi antenna array

The prediction of pulse radiation characteristics of Vivaldi antenna array primarily relies on the spatial superposition of the radiation field of each element antenna, in which the array factor has been incorporated. To differentiate with the aforementioned spatial superposition, the new spatial superposition in this step is referred as the quadratic spatial superposition. Assuming a $M{\times}N$ Vivaldi antenna array with a relative delay sequence between excitation pulses of each element represented by matrix τ, the radiation field waveform at any field point of the array can be obtained using the quadratic spatial superposition:

$$\overrightarrow{E}_{AC}\left(\overrightarrow{r},t\right)=\sum_{i=1,j=1}^{M,N}\overrightarrow{E}_{i,j}\left(\overrightarrow{r}_{i,j},t-\tau_{i,j}\right),\qquad(10)$$

where $\overrightarrow{r}_{i,j}$ stands out the position vector of the field point $\overrightarrow{r}$ with respect to the (i,j) element, $\overrightarrow{E}_{i,j}$ refers to the radiated electric field of the (i,j) element antenna.

For cost reasons, numerical simulation is employed to validate the prediction method to the pulse radiation characteristics of antenna array. A $6{\times}12$ array is constructed using the antipodal Vivaldi antenna in previous part as the array element, as shown in Fig. 18, with spacing of 250 mm in E-plane between each element and spacing of 200 mm in H-plane.

The excitation pulse of each element in the array remains as the measured output waveform from the pulse generator, as depicted in Fig. 15. First consider synchronous excitation, where the time delay sequence matrix is set to zero. The theoretical prediction approach is utilized to obtain the radiated waveforms at the distance of 10 m along the main axis of the array antenna, as illustrated in Fig. 19, and then a comparison is made with numerical results acquired by finite integral techniques. Additionally, Fig. 20 presents the predicted temporal patterns for both E-plane and H-plane under synchronous excitation of the Vivaldi antenna array.

As observed in Fig. 19, the theoretical predicted electric field waveform exhibits excellent agreement with the numerical results, which indicates that the proposed prediction method is capable of achieving accurate predictions for the array antenna radiation field wave-
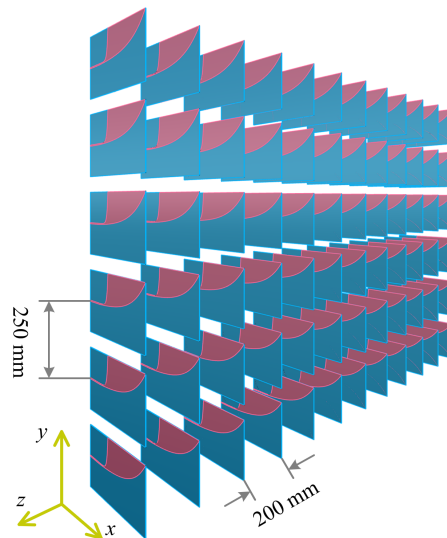

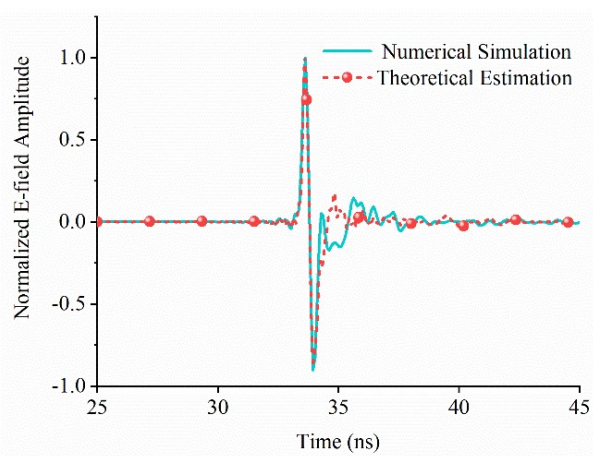Fig. 18. A $6{\times}12$ Vivaldi antenna array.

Fig. 19. Radiated waveforms at 10 m along the main axis of the Vivaldi antenna array.

form. In fact, this outcome is inevitable due to ideal conditions where the waveforms at the main axis field point of an array antenna are essentially identical to those of a single antenna under synchronous excitation. The array antenna beam exhibits a higher degree of concentration and achieves greater gain compared to an individual antenna array element, therefore, it places greater emphasis on its time domain pattern. As depicted in Fig. 20, it can be clearly observed that the theoretically predicted patterns in both E-plane and H-plane for the array antenna align closely with numerical results across a wide range of angles. Notably for the concerned 3-dB beam width, the errors remain below 5%. These findings demonstrate that the proposed theoretical approach also yields effective predictions for the time domain pattern of the Vivaldi antenna array.
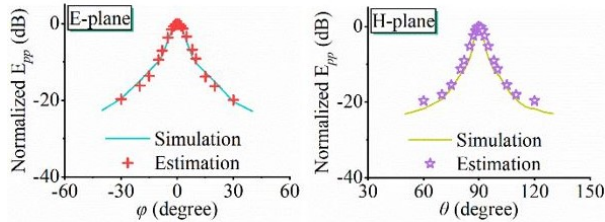
Fig. 20. Temporal patterns of the Vivaldi antenna array in E-plane and H-plane under synchronous excitation.

The beam width of the antenna is determined by the size of the radiating aperture. As evident from both the array aperture dimension and the obtained time-domain patterns, the temporal pattern of the 6×12 array in H-plane appears relatively narrow, necessitating beam scanning in most application scenarios. Beam scanning operates on the principle of configuring the time delay sequence based on the desired scanning angle and spacing between array elements, thereby controlling the excitation timing for each element within the array to deflect the radiation beam, ensuring optimal spatial superposition at the desired angle. Here, employing the theoretical prediction method to obtain the H-plane temporal patterns in different scanning angles, compared with the numerical results, is depicted in Fig. 21.
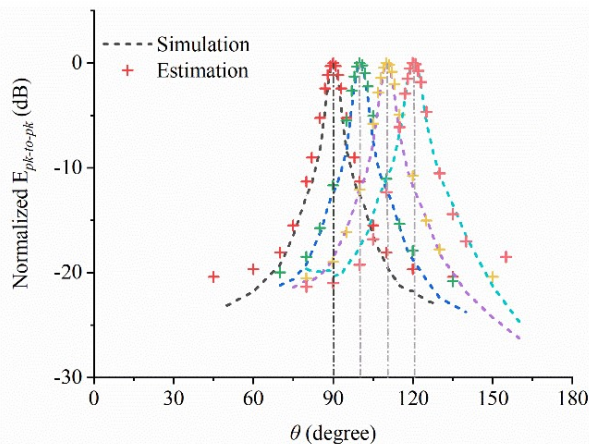

Fig. 21. Temporal patterns on H-plane within different scanning angles.

As demonstrated in Fig. 21, the time-domain pattern of the array can still be effectively predicted when operating in the beam scanning mode, which further validates the correctness and effectiveness of the proposed theoretical prediction method. Based on the proposed prediction method, the time-domain radiation characteristics of the array under different excitation delay sequences can be thoroughly studied and analyzed, leading to significant cost reduction and facilitating the

design, development and engineering implementation of array antennas. Moreover, the issues of pattern synthesis for antenna arrays become feasible by integrating global optimization algorithms and the proposed prediction method. This approach can offer guidance and convenience for radiation characteristics measurements of array via advance prediction.

IV. CONCLUSION

Vivaldi antenna is a widely used ultra-wideband pulse radiating antenna. Estimating the time-domain radiation characteristics of Vivaldi antennas holds significant importance for antenna design, array development and engineering realization. This paper presents a theoretical method for predicting the radiation characteristics of Vivaldi antennas in time-domain, in which the dipole array is employed to model the Vivaldi antenna. By superimposing the pulsed radiation electric fields of dipole antennas, the time-domain radiated field of Vivaldi antenna is obtained. The influence of the construction way and element number of the dipole array on the estimation effect of Vivaldi antenna radiation field in time-domain is investigated, and the specific implementation process of the theoretical estimation method is presented. Additionally, quadratic spatial superposition is employed to incorporate the array factor, enabling the realization of pulsed radiation characteristics of the Vivaldi antenna array. The measurement of a fabricated antipodal Vivaldi antenna is conducted, which demonstrates that the proposed dipole array-based method can accurately predict the radiation field waveform of the Vivaldi antenna. Furthermore, numerical simulation to the Vivaldi antenna array also indicates that this approach effectively enables estimation of radiation field waveform and time-domain patterns of Vivaldi array operating on synchronous excitation and beam scanning mode. This methodology serves as a foundation for array temporal pattern synthesize and contributes to designing and characteristics measurements of the Vivaldi array.

REFERENCES

[1] P. J. Gibson, "The Vivaldi aerial," *IEEE 9th European Microwave Conference*, Brighton, UK, pp. 101-105, Sep. 1979.

[2] A. Hossain and A. V. Pham, "A novel gain-enhanced miniaturized and lightweight Vivaldi antenna," *IEEE Trans. Antennas Propagat.*, vol. 71, no. 12, pp. 9431-9439, Dec. 2023.

[3] Z. Qiao, Z. Wang, T. Loh, S. Gao, and J. Miao, "A compact minimally invasive antenna for OTA testing," *IEEE Antennas Wirel. Propag. Lett.*, vol. 18, no. 7, pp. 1381-1385, July 2019.

[4] R. Cicchetti, V. Cicchetti, A. Faraone, L. Foged, and O. Testa, "A compact high-gain wideband lens

Vivaldi antenna for wireless communications and through-the-wall imaging," *IEEE Trans. Antennas Propagat.*, vol. 69, no. 6, pp. 3177-3192, June 2021.

[5] N. O. Parchin, M. Shen, and G. F. Pedersen, "Small-size tapered slot antenna (TSA) design for use in 5G phased array applications," *Appl. Comput. Electromagn. Soc. J.*, vol. 32, no. 3, pp. 193-202, Mar. 2017.

[6] F. B. Zarrabi, N. P. Gandji, R. Ahmadian, H. Kuhestani, and Z. Mansouri, "Modification of Vivaldi antenna for 2-18 GHz UWB application with substrate integration waveguide structure and comb slots," *Appl. Comput. Electromagn. Soc. J.*, vol. 30, no. 8, pp. 844-849, Aug. 2017.

[7] B. Biswas, R. Ghatak, and D. R. Poddar, "A fern fractal leaf inspired wideband antipodal Vivaldi antenna for microwave imaging system," *IEEE Trans. Antennas Propagat.*, vol. 65, no. 11, pp. 6126-6129, Nov. 2017.

[8] S. M. Kameli, S. S. Refaat, H. Abu-Rub, A. Darwish, A. Ghrayeb, and M. Olesz, "Ultra-wideband Vivaldi antenna with an integrated noise-rejecting parasitic notch filter for online partial discharge detection," *IEEE Trans. Instrum. Meas.*, vol. 73, pp. 1-10, 2024.

[9] B. Wang, H. Ning, Y. Yan, C. Cao, and Q. Liu, "Antipodal Vivaldi antenna with resistance loading on bent terminal," *Int. Conf. Microw. Millim. Wave Technol., ICMMT - Proc.*, Harbin, CN, pp. 1-3, Aug. 2022.

[10] A. S. Dixit, S. Kumar, S. Urooj, and A. Malibari, "A highly compact antipodal Vivaldi antenna array for 5G millimeter wave applications," *Sensors*, vol. 21, no. 7, pp. 2360(1-15), Mar. 2021.

[11] J. Zhang, H. Lan, M. Liu, and Y. Yang, "A handheld Nano through-wall radar locating with the gain-enhanced Vivaldi antenna," *IEEE Sens. J.*, vol. 20, no. 8, pp. 4420-4429, Apr. 2020.

[12] Z. Hu, Z. Zeng, K. Wang, W. Feng, J. Zhang, Q. Lu, and X. Kang, "Design and analysis of a UWB MIMO radar system with miniaturized Vivaldi antenna for through-wall imaging," *Remote Sensing*, vol. 11, no. 16, pp. 1867(1-20), Aug. 2019.

[13] Z. Tahar, X. Derobert, and M. Benslama, "An ultra-wideband modified Vivaldi antenna applied to through the ground and wall Imaging," *Prog. Electromagn. Res. C*, vol. 86, pp. 111-122, Aug. 2018.

[14] D. N. Elsheakh and E. A. Abdallah, "Compact ultra-wideband Vivaldi antenna for ground-penetrating radar detection applications," *Microw.*

Opt. Technol. Lett., vol. 61, no. 5, pp. 1268-1277, Feb. 2019.

[15] J. Zhang, X. Zhang, and S. Xiao, "Antipodal Vivaldi antenna to detect UHF signals that leaked out of the joint of a transformer," *Int. J. Antennas Propag.*, vol. 2017, pp. 1-13, June 2017.

[16] M. Ren, Z. Cheng, L. Wu, H. Zhang, S. Zhang, X. Chen, D. Xing, and H. Qin, "Portable microwave-acoustic coaxial thermoacoustic probe with miniaturized Vivaldi antennas for breast tumor screening," *IEEE Trans. Biomed. Eng.*, vol. 70, no. 1, pp. 175-181, Jan. 2023.

[17] A. M. de Oliveira, A. M. de Oliveira Neto, M. B. Perotoni, N. Nurhayati, H. Baudrand, A. de Carvalho, and J. F. Justo, "A fern antipodal Vivaldi antenna for near-field microwave imaging medical applications," *IEEE Trans. Antennas Propagat.*, vol. 69, no. 12, pp. 8816-8829, Dec. 2021.

[18] U. Rafique, S. Pisa, R. Cicchetti R, O. Testa, and M. Cavagnaro, "Ultra-wideband antennas for biomedical imaging applications: A survey," *Sensors*, vol. 22, no. 9, pp. 3230(1-38), Apr. 2022.

[19] V. M. Fedorov, M. V. Efanov, V. Y. Ostashev, V. P. Tarakanov, and A. V. UI'yanov, "Antenna array with TEM-horn for radiation of high-power ultra-short electromagnetic pulses," *Electronics*, vol. 10, no. 9, pp. 1011(1-18), Apr. 2021.

[20] J. Shao, G. Fang, J. Fan, Y. Ji, and H. Yin, "TEM horn antenna loaded with absorbing material for GPR applications," *IEEE Antennas Wirel. Propag. Lett.*, vol. 13, pp. 523-527, Mar. 2014.

[21] A. Ha, M. H. Chae, and K. Kim, "Beamwidth control of an impulse radiating antenna using a liquid metal reflector," *IEEE Antennas Wirel. Propag. Lett.*, vol. 18, no. 4, pp. 571-575, Apr. 2019.

[22] S. Xiao, S. Altunc, P. Kumar, C. E. Baum, and K. H. Schoenbach, "A reflector antenna for focusing sub-nanosecond pulses in the near field," *IEEE Antennas Wirel. Propag. Lett.*, vol. 9, pp. 12-15, Jan. 2010.

[23] C. Pfeiffer and J. Massman, "An UWB hemispherical Vivaldi array," *IEEE Trans. Antennas Propagat.*, vol. 70, no. 10, pp. 9214-9224, Oct. 2022.

[24] A. M. de Oliveira, J. R. B. Garay, J. P. de Souza, A. M. da Silva, M. B. Perotoni, W. Beccaro, and J. F. Justo, "Active Vivaldi antenna timed-array for ultra-wideband 3D beamforming," *Recent Pat. Eng.*, vol. 10, no. 2, pp. 121-127, Aug. 2016.

[25] X. Jiang, Y. Yan, L. Meng, B. Wang, L. Bi, and Y. Yin, "Theoretical study on directivity of ultra-wideband time-domain antenna array based on 3D impulse point sources," *National Conference on Antennas*, Harbin, CN, pp. 816-818, Aug. 2023.

[26] K. Zhang, L. Wang, R. Liu, M. Wang, C. Fan, H. Zheng, and E. Li, "Low-dispersion leapfrog WCS-FDTD with artificial anisotropy parameters and simulation of hollow dielectric resonator antenna array," *IEEE Trans. Antennas Propagat.*, vol. 69, no. 9, pp. 5801-5811, Sep. 2021.

[27] S. E. Bankov and M. D. Duplenkova, "Transformation of the electromagnetic field in an UWB array of TEM horns," *Proc. IEEE All-Russian Microw. Conf., RMC*, Moscow, RU, pp. 178-181, Nov. 2022.

[28] K. N. Klimov, K. I. Konov, A. M. Belevtsev, I. K. Epaneshnikova, and A. S. Boldyreff, "Electromagnetic modeling of the ultra-wideband antenna array radiator," *Conf. Proc. Radiat. Scatt. Electromagn. Waves, RSEMW*, Divnomorskoe, RU, pp. 232-235, Aug. 2023.

[29] D. M. Pozar, "The active element pattern," *IEEE Trans. Antennas Propagat.*, vol. 42, no. 8, pp. 1176-1178, Aug. 1994.

[30] X. Yang, H. Qian, B. Z. Wang, and S. Xiao, "Radiation pattern computation of pyramidal conformal antenna array with active-element pattern technique," *IEEE Antennas Propag. Mag.*, vol. 53, no. 1, pp. 28-37, Feb. 2011.

[31] M. Zhang, C. Liao, Z. Ye, J. Feng, and Q. Liu, "A rapid method for calculating the pulsed antenna arrays including mutual coupling effects," *Chinese Journal of Radio Science*, vol. 30, no. 5, pp. 864-869, Oct. 2015.

[32] O. V. Mikheev, S. A. Podosenov, K. Y. Sakharov, A. A. Sokolov, and V. A. Turkin, "Approximate calculation methods for pulse radiation of a TEM-horn array," *IEEE Trans. Electromagn. Compat.*, vol. 43, no. 1, Feb. 2001.

[33] B. Wang, Q. Liu, C. Cao, Y. Yan, and T. Jiang, "A method for predicting time-domain radiation characteristics for bowtie antenna," *Int. Appl. Comput. Electromagn. Soc. Symp., ACES-China*, Hangzhou, CN, pp. 1-3, Aug. 2023.

[34] A. Bhattacharjee, A. Bhawal, A. Karmakar, A. Saha, and D. Bhattacharya, "Vivaldi antennas: A historical review and current state of art," *Int. J. Microw. Wirel. Technol.*, vol. 13, no. 8, pp. 833-850, Oct. 2021.

[35] A. S. Arezoomand, R. A. Sadeghzadeh, and M. Naser-Moghadasi, "Novel techniques in tapered slot antenna for linearity phase center and gain enhancement," *IEEE Antennas Wirel. Propag. Lett.*, vol. 16, pp. 270-273, June 2016.

[36] В. И. Кошелев, В. П. Беличенко, and Ю. И. Буянов, "Ultra-wideband electromagnetic radiation technology," National Defense Industry Press, CN, 2018.

Binwen Wang was born in Gansu, China, in 1993. He received his B.S. degree in Nuclear Science from Xi'an Jiaotong University, Xi'an, China, in 2015, and his M.S. degree in Electromagnetic Field and Microwave Techn-ology from the Northwest Institute of Nuclear Techn-ology, Xi'an, China, in 2017. He is currently an Engineer at the Northwest Institute of Nuclear Technology. His research interests include time-domain electromagnetics and ultra-wideband antenna.

Hui Ning was born in Zhejiang, China, in 1969. He received his M.S. and Ph.D. degrees in Nuclear Science and Technology from Tsinghua University, Beijing, China, in 1997 and 2001, respectively. He is currently a Professor at the Northwest Institute of Nuclear Technology, Xi'an, China, specializing in time-domain electromagnetics and the pulse power technique and its applications.

Hao Cai was born in Henan, China, in 1997. He received his B.S. and M.S. degree in Electromagnetic Field and Microwave Technology from the National Defense University of Science and Technology, Chang-sha, China, in 2019 and 2021. He is currently an Engineer at the Northwest Institute of Nuclear Technology, specializing in ultra-wideband pulse generator.

Qilong Liu was born in Hubei, China, in 1997. He received his B.S. degree in Power System and Automation from the Army Engineering University of PLA, Shijiazhuang, China, in 2019. He is currently an Assistant Engineer at the Northwest Institute of Nuclear Technology, specializing in ultra-wideband antenna.

Yan Wang was born in Ningxia, China, in 2000. She received her B.S. degree in Electromagnetic Field and Microwave Technology from the National Defense University of Science and Technology, Chang-sha, China, in 2022. She is currently an Engineer at the Northwest Institute of Nuclear Technology, specializing in ultra-wideband pulse generator.

Youjie Yan was born in Henan, China, in 1982. He received the B.S. degree in electronical information science and technology from Xidian University, Xi'an China, in 2005, the M.S. degree in electromagnetic field and microwave technology from the Northwest Institute of Nuclear Technology, Xi'an, China, in 2008, and the Ph.D. degree in plasma physics from the University of Electronic Science and Technology of China, Chengdu, China. He is currently a Professor level senior engineer. His research interests include the time-domain electromagnetics and the electromagnetic compatibility.